J Mater Sci: Mater Electron (2012) 23:511–519
DOI 10.1007/s10854-011-0429-3

The effect of Pr addition on superconducting and mechanical properties of Bi-2212 superconductors

O. Ozturk · E. Asikuzun · M. Erdem · G. Yildirim · O. Yildiz · C. Terzioglu

Received: 2 March 2011 / Accepted: 6 June 2011 / Published online: 18 June 2011

Abstract In this work, the effects of Pr doping on the superconducting, structural and mechanical properties of the samples are analyzed. Pr doped Bi-2212 superconductors are obtained using solid state reaction method. Dc resistivity measurements are made to investigate the superconducting properties, microhardness measurements are made to analyze the mechanical properties, XRD and SEM measurements are done for crystal structure determination and calculation of the lattice parameters. Using EDS measurements, the change in the elemental composition with doping is analyzed. The Vickers microhardness is calculated for undoped and doped samples. The experimental results of the microhardness measurements are analyzed using Kick's Law, PSR (proportional specimen resistance), modified PRS (MPSR) and Hays–Kendall (HK) approach. The microhardness values of the samples decrease with Pr addition. The results can be successfully explained by HK approach.

1 Introduction

As is well known, chemical doping, addition and diffusion are important for copper based high temperature superconductors. Numerous studies are done about doping of cuprates aiming to enhance their superconducting and mechanical properties [1–3]. In literature, the effect of the addition of various elements instead of Cu, Ca, and Sr on the superconducting and mechanical properties of Bi-2212 high temperature superconductors are analyzed [4–6] and increase in T_c^{onset} and decrease of room temperature resistivities are observed. The studies on Pr addition showed an increase in room temperature resistivity and decrease in the critical temperature (T_c^{onset}) with increasing amount of addition [7–10].

The mechanical properties of superconductors are important for industrial applications. Generally, superconducting applications require superconductors in the form of wires or tapes. Useful superconductors need to be strong, flexible, and ductile as well as having good superconducting properties. Indentation microhardness is a convenient method to investigate the mechanical properties. In this study, Praseodymium (Pr) added Bi-2212 samples are prepared using solid state reaction method. XRD, SEM, EDS, electrical resistivity (*R–T*) and Vickers microhardness measurements are made to investigate the effect of Pr addition on the superconducting and mechanical properties of the samples.

2 Experimental techniques

To produce Pr added Bi-2212 samples, Pr_2O_3 powder was added at 0.1, 0.2, 0.3, 0.5, 0.7, and 1% ratios. The resultant powder was ground for 4 h to obtain a homogeneous sample and then pressed at 10 tons to obtain pellets 13 mm in diameter and 1–1.5 mm in thickness. The pellets were put into a tube furnace and heated to an optimum temperature of 840 °C with 10 °C/min. They are kept at this temperature for 50 h and cooled down to room temperature with 3 °C/min.

O. Ozturk (✉) · E. Asikuzun · O. Yildiz
Department of Physics, Faculty of Arts and Science, Kastamonu University, 37100 Kastamonu, Turkey
e-mail: oozturk@kastamonu.edu.tr

M. Erdem · G. Yildirim · C. Terzioglu
Department of Physics, Faculty of Arts and Science, Abant Izzet Baysal University, 14280 Bolu, Turkey

For transport measurements, four-point contacts are made with silver paste. The resistivities of the samples as a function of temperature are measured in a cryostat using 5 mA direct current in the temperature range 25–120 K with 5 K/min cooling and heating rates. The transition temperature (T_c^{onset}) is decided as the critical temperature where the resistance decreased and superconductivity started. To investigate the surface structure, possible accumulation at the grain boundaries and the grain sizes, SEM analyses were made. XRD measurements are made to calculate the crystal structure and crystal parameters. Moreover, EDS (Energy dispersive spectrometer) is used to all samples investigate the change in ion quantity with addition. Vickers microhardness measurements are made on the sample surfaces at room temperature to investigate the effect of Pr addition on the mechanical properties using a digital microhardness tester (SHIMADZU). The load was applied for 10 s and changed in the range 0.245–2.940 N. The indentations were made at different regions of the sample surfaces making sure that the indentations do not overlap.

3 Results and discussion

3.1 XRD analyses

The undoped Bi-2212 sample is called *Pure*, and Pr added samples are called *Pr0.1, Pr0.3, Pr0.5, Pr0.7* and *Pr1.0,* respectively. In Fig. 1, the XRD graphs of the samples are shown. The crytal parameters are calculated using least squres method from XRD graph and are tabulated in Table 1. Increasing the amount of Pr decreases the volume fraction of 2212 phase and increases that of 2201 phase. The dominant phase is the 2212 phase. With Pr addition, the *a* parameter icreases and the *c* parameter decreases. This result shows the majority of the resultant phase is Bi-2212 and Pr ions enter into the crystal structure of Bi-2212 superconductor [7, 11].

The XRD peak belonging to (008) plane is shown in Fig. 2. The peaks shift to higher angles with Pr addition. This shift shows that the *c* parameter decreases with increasing Pr addition. The change in *c* parameter is due to the insertion of the majority of the dopant rare earth elements into the crystal structure [6, 11, 12].

In high temperature superconductors, the exchange of +3 valency rare earths with +2 valency Sr or Ca results in an increase in the oxygen content due to the added electron in the system. The excess oxygen is taken by oxygen deficient Bi–O double planes. This results in a decrease in the positive charge in Bi–O planes so the repelling force between positive charges decreases and the connections will be tighter. As a result, the sizes of Bi–O planes and the length of the *c* parameter decrease. Moreover, when the radius of the added ion is smaller than that of Sr (1.12 Å) the *c* parameter is expected to decrease. Systematic increase in the *a* parameter is observed with Pr (1.013 Å) addition. This is an expected result due to extra electrons arising with Pr addition. The effective valency of Cu decreases which results in an increase in Cu–O bond length and thus the *a* parameter also increases [13–15].

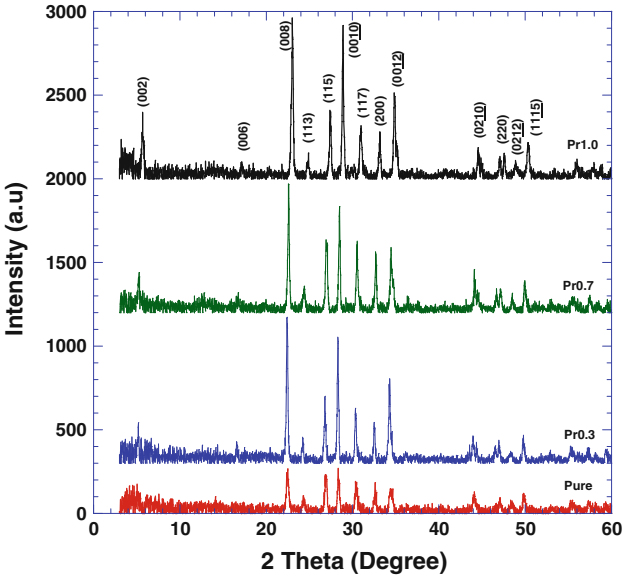

Fig. 1 XRD patterns of the Pure, Pr0.3, Pr0.7 and Pr1.0 samples

3.2 Carrier concentration calculation

It is known that the transition temperature in high temperature superconductors depends on the density of mobile holes in the CuO_2 planes. As stated above, replacement of Sr^{2+} or Ca^{2+} with Pr^{3+} is expected to decrease the hole concentration in the system.

The carrier concentration, *p*, is calculated by using the relation,

$$T_c/T_c^{max} = 1 - 82.6(p - 0.16)^2 \quad (1)$$

where T_c^{max} is taken as 85 K for Bi-2212 system [16]. The calculated carrier concentrations of the samples are summarized in Table 1. It is observed that the hole carrier concentration decreases with increasing Pr doping level.

3.3 Grain size calculation

One of the important calculations based on XRD analyses is the calculation of grain sizes. This can be made using the FWHM (full width at half maximum) of the peaks and the relation;

$$D = 0.94\lambda/\beta\cos\theta \quad (2)$$

Table 1 Some characteristics of superconducting samples

Samples	a (Å)	c (Å)	Volume fraction (%) 2212–2201	T_c^{onset}–T_c^{offset} (K)	Resistivity at 300 K (Ω mm)	Hole concentration p	Grain size (Å)
Pure	5.40	30.80	90.0–10.0	87.0–76.0	0.0047	0.125	4.643
Pr0.1	5.41	30.78	89.0–11.0	94.0–75.0	0.0060	0.122	4.594
Pr0.3	5.44	30.76	87.6–12.4	95.0–72.0	0.0074	0.116	3.960
Pr0.5	5.45	30.75	86.2–13.8	95.5–71.0	0.0075	0.115	3.334
Pr0.7	5.48	30.71	82.1–17.9	96.0–71.0	0.0076	0.115	3.292
Pr1.0	5.49	30.70	80.8–19.2	97.0–70.0	0.0079	0.113	3.280

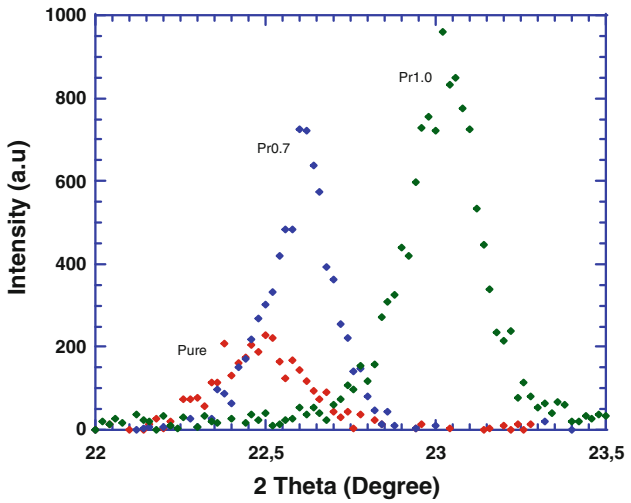

Fig. 2 XRD peaks for the (008) plane

where β is FWHM value for a characteristic peak. The calculated grain sizes are tabulated in Table 1. As can be seen from the table, the grain sizes decrease with Pr addition a result which is supported by the SEM results.

3.4 SEM and EDS analyses

Flaky grains which are common in Bi-2212 high temperature superconductors are seen both for pure and Pr added samples. Figure 3 shows that the grain sizes decrease and porosity increases with doping. When Pure and Pr1.0 samples are compared, the grains of the Pr1.0 sample are smaller and the surface is more porous. As a result, there is no enhancement in the surface structure due to Pr addition.

For all samples with and without addition, energy dispersive spectrometer is used to analyze the ion amount due to addition. In Fig. 4, the change in ion amounts due to addition is shown. The density of Sr decreases associated with an increase in Pr density. A small decrease is also seen in Ca groups. But the decrease in Sr is more pronounced. These results show that Sr atoms are replaced by Pr atoms in Bi-2212 structure [4].

3.5 Electrical resistivity measurements

The variation of resistivity with temperature for all samples are given in Fig. 5. All samples show metallic behaviour above T_c^{onset} temperature. The values of T_c^{onset}, and resistivity ρ are given in Table 1.

The T_c^{onset} is 87 K for the pure sample and the T_c^{onset} value increases monotically with Pr addition. The T_c^{offset} value of the pure sample is 76 K and it decreases monotically with Pr addition. This behaviour is shown in Fig. 5. The room temperature resistivity increases with Pr addition. The grain sizes decrease with Pr addition and so the increase in the number of contacts between grains increases the resisitivity. The superconducting transition gap ΔT increases in doped samples when compared to the pure sample as shown in Fig. 5. This is due to the higher impurity levels and lattice defects of the doped samples [5].

3.6 Microhardness and modelling

The load dependent (Vickers) microhardness values of the samples are calculated using the relation;

$$H_v = 1854.4\left(F/d^2\right) \tag{3}$$

where F is the applied load in N and d is the diagonal length of the indentation mark in μm. From the microhardness measurement results, it is observed that the load dependent microhardness values decrease with applied load for all samples as shown in Fig. 6. The variation of load dependent microhardness has a similar shape for all samples. Quinn and Quinn (1997) [17] analyzed the load dependent Vickers microhardness of various ceramic samples and they observed a smooth convergence of the hardness- load curves to a plateau of constant hardness value. They claimed that the value of the hardness at the plateau region gives the real hardness value. For higher values of applied load, the microhardness values saturate in the plateu region. In this region the dependence of microhardness to the applied load is weak. In the proceeding sections, the values of microhardness in this plateu region

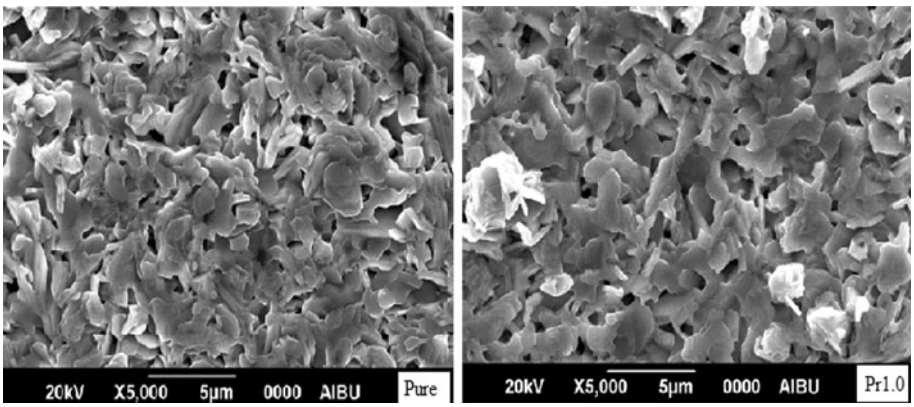

Fig. 3 SEM micrograph of Pure and Pr1.0 samples

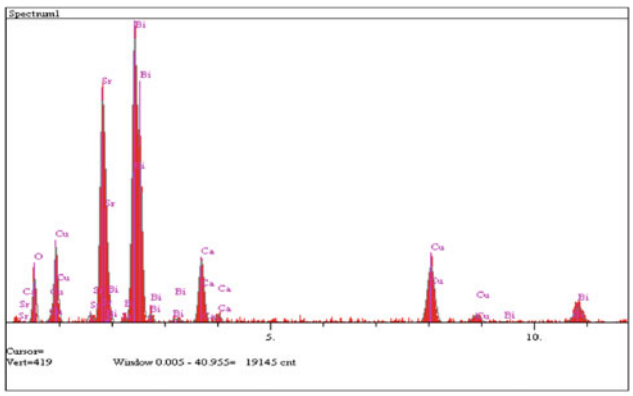

(a) Pure

Elt.	Intensity (c/s)	Conc.
O	15.11	13.502
Ca	29.14	3.931
Cu	37.69	11.863
Sr	78.79	26.028
Bi	12.96	44.676
		100.000

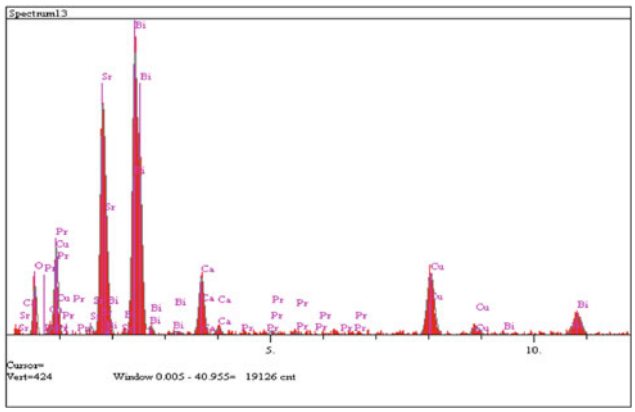

(b) Pr1.0

Elt.	Intensity (c/s)	Conc.
O	14.08	13.152
Ca	24.59	3.519
Cu	34.71	11.580
Sr	70.14	24.915
Pr	1.95	1.402
Bi	12.46	45.438
		100.000

Fig. 4 EDS patterns of **a** Pure, **b** Pr1.0 samples

are used for comparison with several proposed models to calculate load independent microhardness. The undoped (pure) sample has the highest microhardness values for all values of applied load. With increasing amount of doping level the microhardness values decrease monotically. The decrease of microhardness with doping can be explained by the formation of impurities and irregularities and to the increase in porosity as observed in SEM measurements. The nonlinear relation between applied load and microhardness is observed in similar studies [18–24]. In literature, several models are proposed to calculate the load independent microhardness and to explain ISE (indentation size effect). These models are used in this study to calculate load independent microhardness values for all samples [18, 19].

3.6.1 Analysis according to Meyer's law

One of the commonly used relations to explain ISE is Meyer's law [17].

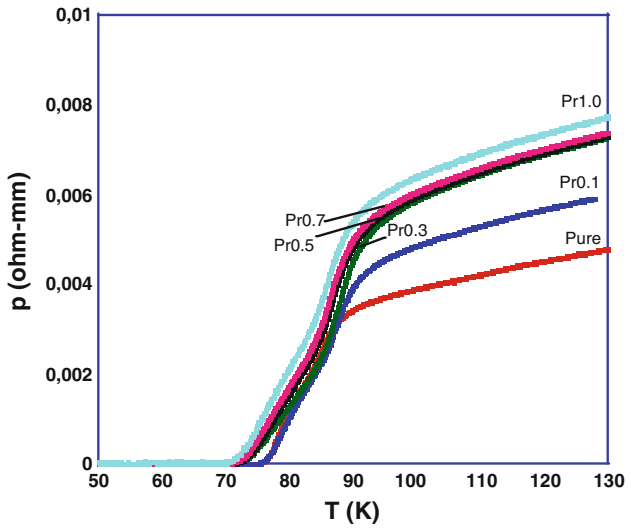

Fig. 5 Resistivity as a function of temperature curves for the samples

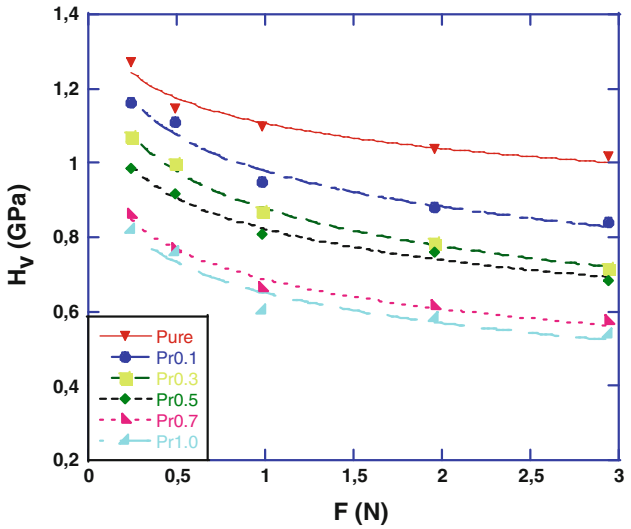

Fig. 6 Variation of load dependent microhardness H_v with applied load F

$$F = Ad^n \tag{4}$$

where n is Meyer number which is obtained from the fitted curves of the experimental data. The slope of the ln F-ln d graph gives n_k, and the vertical intercept is A_{1K}. The linear relation in the graph shows that Meyer's law is suitable for the calculation of microhardness values using PRS model, MPRS model and Hays Kendall approach. The values of LRC, ln A_{1K} and n_K obtained from Fig. 7 are tabulated in Table 2. The value of Meyer number decreases with Pr addition. This result also shows that microhardness decreases with Pr addition since for lower values of n, an applied load F produces longer indentations (d). The value of Meyer number is less than 2 for the samples which

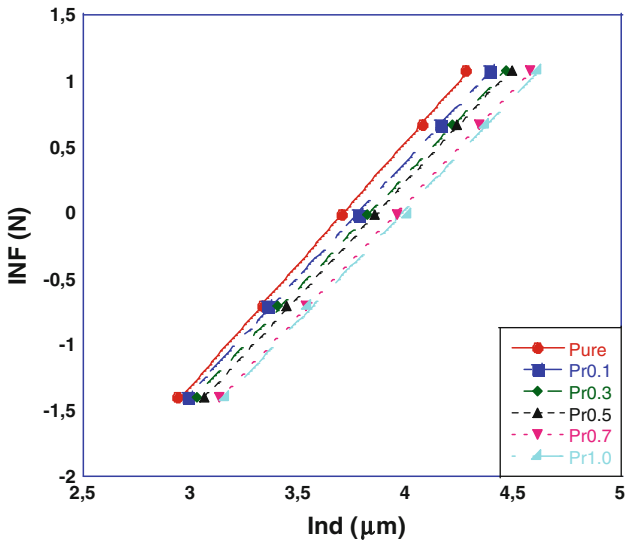

Fig. 7 Variation of applied load ln$F$ with diagonal ln$d$ for the samples

Table 2 Best-fit results of experimental data according to Meyer's law

Samples	Meyer number n_k	InA_{1K} (GPa)	Regression coefficient (R)
Pure	1.856	−6.885	0.99972
Pr0.1	1.753	−6.624	0.99978
Pr0.3	1.718	−6.586	0.99988
Pr0.5	1.745	−6.745	0.99985
Pr0.7	1.718	−6.797	0.99993
Pr1.0	1.698	−6.766	0.99937

proves that the load dependent displacement is via ISE behaviour.

3.6.2 Analysis according to PSR model

An alternative to analyze ISE behaviour is the proportional sample resistance (PSR) model.

$$F/d = W_{PSR} + A_{1PSR}d \tag{5}$$

The hardness value according to PSR model can be calculated using

$$H_v = 1854.4A_{1PSR} \tag{6}$$

The variation of F/d versus d of the samples are given in Fig. 8. The calculated values of load independent microhardness values are given in Table 3. The microhardness values decrease with Pr addition. The load independent hardness values of the samples calculated using PSR model are lower than the values of the plateu region. As seen from the figure, there is prominent divergence from linearity

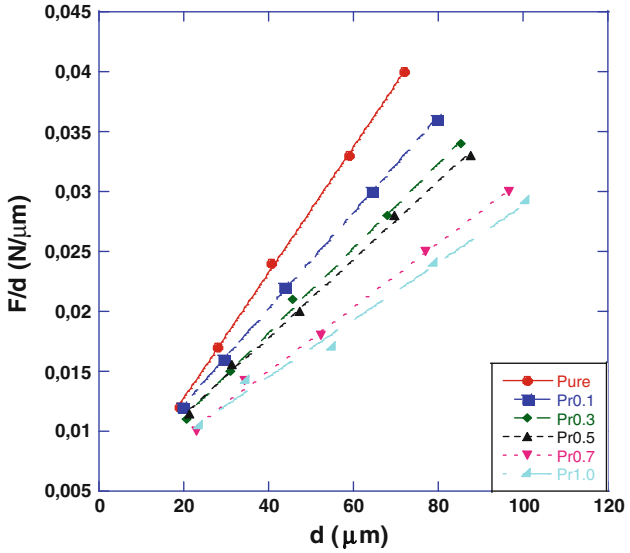

Fig. 8 Plots of *F/d* versus *d* for the samples

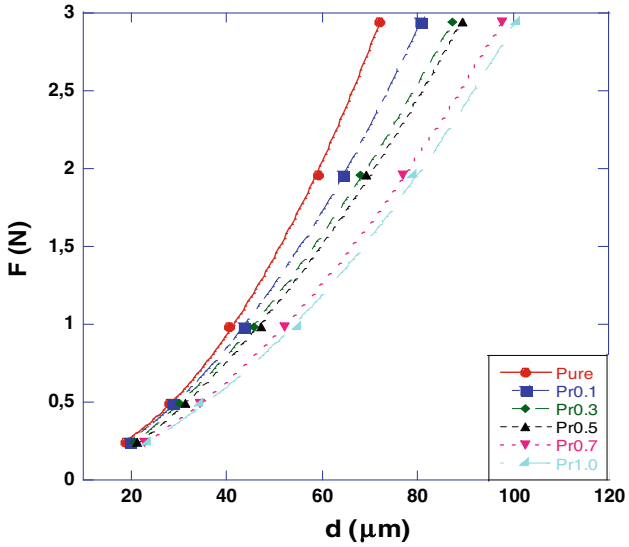

Fig. 9 Variation of applied load with the indentation diagonal length for the samples

especially for higher concentrations of Pr doping. Moreover, the calculated load dependent microhardness value is far from the load independent microhardness value calculated using PSR model. Therefore, it is clear that PSR model is not adequate for determination of the real microhardness value of BSCCO polycrytals.

3.6.3 Analysis according to modified PSR (MPSR) model

According to this model, the physical meaning of $A_{0\mathrm{MPRS}}$ and $A_{1\mathrm{MPRS}}$ parameters are the same as the ones in PSR model [17].

$$F = W_{\mathrm{MPSR}} + A_{0\mathrm{MPRS}}d + A_{1\mathrm{MPRS}}d^2 \tag{7}$$

The values of $A_{0\mathrm{MPRS}}$ and $A_{1\mathrm{MPRS}}$ are obtained from *F–d* graph as shown in Fig. 9. Using MPSR model, the load independent hardness values are calculated as,

$$H_{\mathrm{MPSR}} = 1854.4A_{\mathrm{MPSR}} \tag{8}$$

The values of W_{MPSR}, $A_{0\mathrm{MPSR}}$, $A_{1\mathrm{PSR}}$ and LRC and associated load independent hardness values are given in Table 4. As seen in the table, the values of load independent hardness calculated using MPSR model are also far from the values of the plateau region.

3.6.4 Analysis using Hays–Kendall approach

Hays–Kendall (1973) suggested that the experimentally measured indentation size is proportional to an effective load $F_{\mathrm{eff}} = F - W_{\mathrm{HK}}$ instead of the applied load F [20].

$$F - W_{\mathrm{HK}} = A_{1\mathrm{HK}}d^2 \tag{9}$$

In Fig. 10, the correlation coefficients of the graph of the samples are very high. As seen from the figure, the W_{HK} value (*y*-intercept of the graph) needed to generate the initial deformation increases with doping level. For this model the load independent hardness value is calculated using;

$$H_{\mathrm{LHK}} = 1854.4A_{1\mathrm{HK}} \tag{10}$$

The slope of the curve in Fig. 10 gives the value of $A_{1\mathrm{HK}}$. In Table 5 the values of load independent hardness values, W_{HK}, n_{HK}, and LRC are given. The load independent microhardness value decreases monotically with Pr

Table 3 Best-fit results of experimental data according to PSR model

Samples	$W_{\mathrm{PSR}} \times 10^{-3}$ (N)	$A_{1\mathrm{PSR}} \times 10^{-5}$ (N/μm)	R	Load independent hardness H_{PSR} (GPa)	Load dependent hardness (in plateau region) H_{V} (GPa)
Pure	2.25	52.43	0.99972	0.972	1.018–1.038
Pr0.1	4.23	40.04	0.99987	0.742	0.841–0.879
Pr0.3	4.10	35.29	0.99884	0.654	0.715–0.786
Pr0.5	4.88	32.44	0.99855	0.601	0.682–0.760
Pr0.7	4.35	26.65	0.99832	0.494	0.573–0.613
Pr1.0	5.00	23.82	0.99510	0.441	0.537–0.581

Table 4 Best-fit results of experimental data according to MPSR model

Samples	W_{MPSR} (N)	$A_{0MPSR} \times 10^{-5}$ (N/μm)	$A_{1MPSR} \times 10^{-5}$ (N/μm^2)	R	Load independent hardness H_{MPSR} (GPa)	Load dependent hardness H_V (GPa)
Pure	0.080	−174.4	57.51	0.99985	1.066	1.018–1.038
Pr0.1	−0.038	746.9	36.65	0.99996	0.679	0.841–0.879
Pr0.3	−0.155	1402.1	24.66	0.99999	0.457	0.715–0.786
Pr0.5	−0.178	1408.3	23.48	0.99966	0.435	0.682–0.760
Pr0.7	−0.070	824.6	23.26	0.99994	0.431	0.573–0.613
Pr1.0	−0.036	674.7	22.78	0.99961	0.422	0.537–0.581

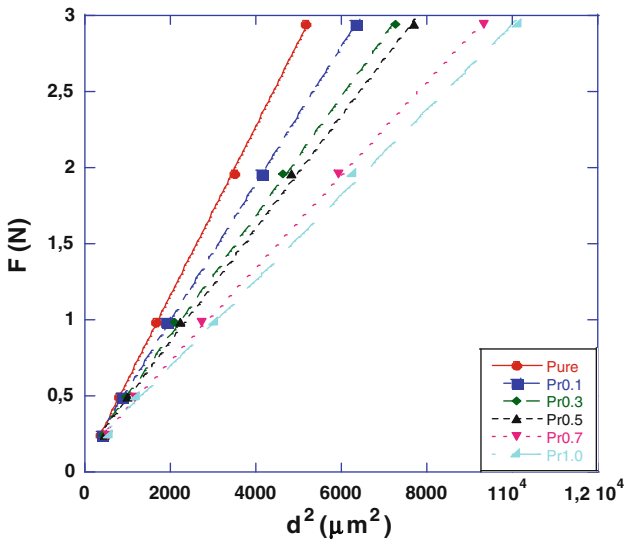

Fig. 10 Applied load versus the square of the impression semi-diagonal length for the samples

addition. The value of n_{HK} is higher than 2 which shows that the load independent microhardness value calculated from HK model reached to the plateau region where the hardness becomes load independent. In HK approach, the graph shows excellent linearity with high regression coefficents implying that it successfully describes the indentation data of the samples.

The results of the hardness values for PSR, MPSR, and HK models are given along with Vickers microhardness values of the samples in the plateu region in Table 6 for comparison. The addition of Pr decreases Vickers microhardness values of the samples as seen in Fig. 11, similar behaviour is observed for all compared models. As a result, the load independent microhardness value calculated using HK approach gives closer results to the ones in the plateau region when compared to the PSR and MPSR models. In literature it is stated that the load independent microhardness values should converge to the values of the plateau region [18–24]. Since the experimental results have high correlation and the calculated load independent microhardness value converge to the one in the plateau region, Hays–Kendall model is the most suitable one for the calculation of microhardness of the samples used in this study.

4 Conclusions

The effect of Pr doping on the mechanical and superconducting properties of Bi-2212 is analysed. To determine the mechanical properties, the results of the microhardness measuremenets are analyzed using Kick's law, PSR, MPRS, and Hays–Kendal approach and the following results are obtained:

- Room temperature resistivity increased with Pr doping level.
- The superconducting transition temperature (T_C^{onset}) increased with Pr doping level.

Table 5 Best-fit results of experimental data according to HK model

Samples	Load independent hardness constant A_{1HK}(GPa)	W_{HK} (N)	R	n_{HK}	LRC	Load independent hardness H_{LHK} (GPa)	H_V (GPa)
Pure	55.64×10^{-5}	0.046	0.99983	1.994	0.99993	1.031	1.018–1.038
Pr0.1	45.06×10^{-5}	0.093	0.99987	2.048	0.99775	0.835	0.841–0.879
Pr0.3	39.18×10^{-5}	0.117	0.99945	2.110	0.99588	0.726	0.715–0.786
Pr0.5	37.06×10^{-5}	0.119	0.99938	2.154	0.99597	0.687	0.682–0.760
Pr0.7	30.52×10^{-5}	0.121	0.99963	2.133	0.99702	0.565	0.573–0.613
Pr1.0	28.08×10^{-5}	0.134	0.99919	2.153	0.99625	0.520	0.537–0.581

Table 6 The results of load dependent Vickers microhardness at the plateu region and load independent hardness values calculated using PSR, MPSR, and HK models

Samples	Load dependent hardness (in plateau region) H_V (GPa)	Load independent hardness H_{PSR} (GPa)	Load independent hardness H_{MPSR} (GPa)	Load independent hardness H_{LHK} (GPa)
Pure	1.018–1.038	0.972	1.066	1.031
Pr0.1	0.841–0.879	0.742	0.679	0.835
Pr0.3	0.715–0.786	0.654	0.457	0.726
Pr0.5	0.682–0.760	0.601	0.435	0.687
Pr0.7	0.573–0.613	0.494	0.431	0.565
Pr1.0	0.537–0.581	0.441	0.422	0.520

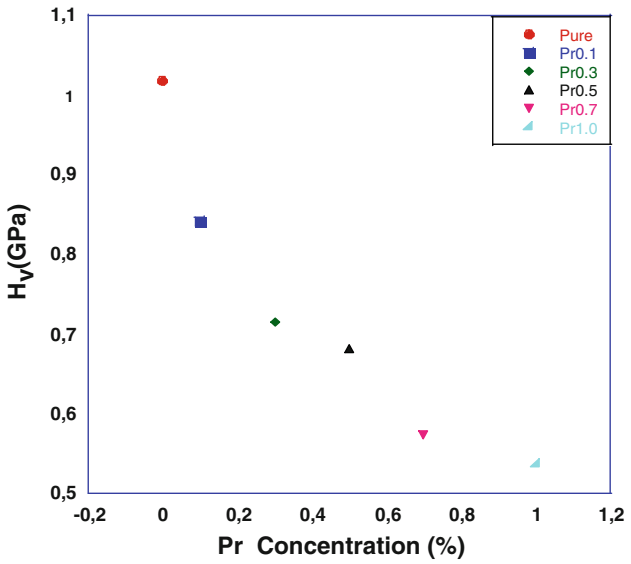

Fig. 11 Variation of load dependent microhardness H_v with Pr concentration

- The reason of the decrease in microhardness value with Pr doping could be the structure of the impurity phases and the irregularities in the grain boundaries. These factors lead to the decrease in the bond strengths causing decrease in the microhardness.
- There is no obvious secondary phase in the XRD results. This result shows that the majority of Pr atoms enter into the Bi-2212 crystal structure.
- SEM results show that the grain sizes decrease with Pr doping and the porosity increases, The decrease in the microhardness values is associated with the increase in the porosity between the grains.
- From the EDS analyses, the Sr percentage in Pr1.0 sample decreases and this decrease is more than that of the other atoms when compared to the pure sample. This means Pr^{3+} ions mainly replace Sr^{2+} ions. The increase in the oxygen content and the difference in the ionic radii between Pr^{3+} (1.013 Å) and Sr^{2+} (1.120 Å) are significant factors of atomic substitutions.
- The experimental results of the microhardness measurements are analysed using Kick's law, PSR, MPSR and Hays–Kendal approach and the acceptable results obtained with HK approach.

References

1. O. Ozturk, M. Akdogan, H. Aydın, M. Yilmazlar, C. Terzioglu, I. Belenli, Phys. B **399**, 94–100 (2007)
2. M. Yilmazlar, O. Ozturk, O. Gorur, I. Belenli, C. Terzioglu, Supercond. Sci. Technol. **20**, 365–371 (2007)
3. C. Terzioglu, O. Ozturk, I. Belenli, J. Alloys Compounds **471**, 142–146 (2008)
4. A. Biju, U. Syamaprasad, R. Ashok, J.G. Xu, K.M. Sivakumar, Y.K. Kuo, Phys. C **466**, 69–75 (2007)
5. A. Biju, P.M. Sarun, R.P. Aloysius, U. Syamaprasad, J. Alloys Compounds **454**, 46–51 (2008)
6. S. Vinu, P.M. Sarun, R. Shabna, A. Biju, U. Syamaprasad, Mater. Lett. **62**, 4421–4424 (2008)
7. X. Sun, X. Zhao, W. Wu, X. Fan, X.-G. Li, H.C. Ku, Phys. C **307**, 67–73 (1998)
8. Q. Cao, K.Q. Ruan, S.Y. Li, X.H. Chen, G.G. Qian, L.Z. Cao, Phys. C **334**, 237–242 (2000)
9. C.A.M. Dos Santos, S. Moehlecke, Y. Kopelevich, A.J.S. Machado, Phys. C **390**, 21–26 (2003)
10. N. Boussouf, M.-F. Mosbah, T. Guerfi, F. Bouaïcha, S. Chamekh, A. Amira, Phys. Proc. **2**, 1153–1157 (2009)
11. S.Vinu, P.M. Sarun, A. Biju, R. Shabna, P. Guruswamy, U. Syamaprasad, Supercond. Sci. Technol. **21**, 045001 (2008)
12. R. Shabna, P.M. Sarun, S. Vinu, A. Biju, U. Syamaprasad, Supercond. Sci. Technol. **22**, 045016 (2009)
13. M.A. Aksan, M.E. Yakinci, J. Mater. Process. Technol. **196**, 365–372 (2008)
14. M. Yilmazlar, H.A.Cetinkara, M. Nursoy, O. Ozturk, C. Terzioglu, Phys. C **442**, 101–107 (2006)
15. C. Terzioglu, H. Aydın, O. Ozturk, E. Bekiroglu, I. Belenli, Phys. B Condens. Matter **403**, 3354–3359 (2008)
16. T. Kucukomeroglu, E. Bacaksiz, C. Terzioglu, A. Varilci, Thin Solid Films **516**, 2913–2916 (2008)
17. J.B. Quınn, V.D. Quınn, J. Mater. Sci. **32**, 4331–4346 (1997)
18. C. Terzioglu, J. Alloys Compounds **509**, 87–93 (2011)

19. O. Sahin, O. Uzun, M. Sopicka-Lizer, H. Gocmez, U. Kölemen, J. Eur. Ceramic Soc. **28**, 1235–1242 (2008)
20. C. Hays, E.G. Kendall, Metall. **6**, 275–282 (1973)
21. J.H. Gong, J.J. Wu, Z. Guan, Mater. Lett. **38**, 197 (1999)
22. J. Gong, Z. Zhao, Z. Guan, H. Mıao, J. Eur. Ceramic Soc. **20**, 1895–1900 (2000)
23. Z. Peng, J. Gong, H. Mıao, J. Eur. Ceramic Soc. **24**, 2193–2201 (2004)
24. U. Kölemen, O. Uzun, M.A. Aksan, N. Güçlü, E. Yakıncı, J. Alloys Compounds **415**, 294–299 (2006)